Sustainable Energy and Artificial Intelligence 2(3) (2026) 145-159 DOI: 10.61186/seai.2605-1052

Hamedan University of Technology

Iranian Association of Electrical and Electronics Engineers

Sustainable Energy and Artificial Intelligence

Online ISSN: 3060-8015

Journal Homepage: www.enai.hut.ac.ir

Design of an Improved Adaptive Fuzzy-FOPID Controller to Enhance Frequency Stability in the TAPS

Farhad Amiri[1*], Mohammad Hassan Moradi[2], Arefe Shalbafian[3]

[1] Department of Electrical Engineering, Tafresh University, Tafresh, 39518-79611, Iran.
[2]Electrical Engineering Department, Faculty of Engineering, Bu-Ali Sina University, Hamedan
[3]Department of Electrical Engineering, Hamedan University of Technology, Hamedan, Iran
** Corresponding Author: f.amiri@tafreshu.ac.ir*

Article Info

Article type:
Original Article

Article history:
Received 2026-05-01;
Revised 2026-05-19;
Accepted 2026-06-02.

How to cite this article:
Amiri, F, Moradi, M H and Shalbafian, A. (2026). Design of an Improved Adaptive Fuzzy-FOPID Controller to Enhance Frequency Stability in the TAPS. (e736747). Sustainable Energy and Artificial Intelligence, 2(3), 145-159. 10.61186/seai.2605-1052

Abstract

Frequency stability is the fundamental problem of keeping the PS's frequency within a reasonable range. The PS's stability would be threatened by frequency variation brought on by load disruptions and uncertainty pertaining to PS characteristics. The PS's LFC system is crucial for controlling and maintaining frequency stability. This work uses the adaptive Fuzzy-FOPID (FFOPID) controller in the LFC structure to address uncertainties and disturbances while improving frequency stability in a two-area PS (TAPS). Additionally, RL has been used to enhance the adaptive FFOPID controller's performance. The adaptive FFOPID controller's performance against the uncertainties and disruptions of the TAPS has been enhanced by RL, which has also increased the control system's environmental adaptability. In a number of scenarios, the suggested control (FFOPID-RL) method has been compared to FFOPID, PDSMC, and SMC control methods. The findings indicate that the control method is better at lowering frequency deviations, settling times, and damping frequency oscillations associated with the TAPS.

Keywords: Fuzzy-FOPID Controller; Adaptive; Frequency Deviation; PS.

Nomenclature

T_{ESS} (s)	The time constant related to the ESS	T_{ESS} (s)	The time constant related to the ESS
LFC	Load-frequency control	MPC	Model Predictive Control
RL	Reinforcement learning	HGSO	hunger games search optimizer
LOA	lyrebird optimization algorithm	OSA	Owl Search Algorithm
SMC	Sliding mode control	FPA	Flower pollination algorithm
PDN-PI	Proportional-derivative with filter and proportional-integral	PD-PI	Proportional derivative-Proportional integral
PDSMC	Proportional-derivative sliding mode control	PSO	Particle swarm optimization

1. Introduction

The capacity of a PS to keep its frequency within a consistent and tolerable range is known as frequency stability [1]. A certain nominal frequency is assigned to each electricity system; in many nations, that frequency generally 50 Hz or 60 Hz [2]. When a PS's frequency stays within the allowable range in spite of fluctuations in demand and disruptions, it is said to be stable [3]. If this stability is compromised, the system will experience problems such as reduced power quality, disruption of sensitive equipment, and even widespread outages [3,4]. Sudden load changes and disturbances are among the main factors of frequency deviation in a PS [5-7]. For example, a sudden increase in load causes the generator turbines to slow down, resulting in a decrease in the frequency of the PS, while a decrease in load can cause an increase in the frequency. In conditions where the frequency deviation exceeds the permissible limit, sensitive equipment is automatically disconnected from the network to prevent possible damage; this leads to further instability and a chain of outages. LFC systems are employed in single-area and multi-area PS architectures to overcome these issues [9-10]. The primary goals of LFC are to coordinate power flows between interconnected areas and to hold the system frequency at its nominal level [11]. By modifying power plant generation, this controller, which functions at the energy generation level, rectifies frequency and power exchange aberrations [12]. In PSs, LFC systems are often deployed in a multi-layered fashion: 1) Primary control 2) Secondary control 3) Tertiary control [11,12].

Using mechanical adjustments to the generators, primary control works locally to try to return the frequency to its starting point [10,11]. This adjustment is fast but usually cannot completely correct the frequency deviations [11]. Secondary control operates centrally as LFC system and compensates for the remaining deviations in frequency that the primary control was unable to completely correct [10,11]. This control is carried out by changing the generation of different power plants and has a slower response time but is more accurate [11]. This layer helps to economically regulate and optimize the generated power so that the system remains cost-effective.

The emergence of new problems in modern PSs highlights the need for advanced LFC control strategies [9,10]. Among these challenges include load disruptions and the unpredictability of PS parameters [9,10]: In PSs, sudden and unforeseen fluctuations in electricity demand are referred to as load disturbances. These changes can directly affect LFC performance and jeopardize the frequency stability of the system [9]. To keep the equilibrium between electricity supply and demand, generators in a PS supply the precise amount of power required [9]. When the load suddenly increases or decreases, this balance is disrupted, causing the PS's frequency to fluctuate and deviate from the nominal value [9,10]. Uncertainties exist in a number of PS characteristics, such as load variations, generator dynamics, and inter-area interactions [9,10]. It is challenging to develop and fine-tune the LFC controller because of these uncertainties [11]. Multiple control approaches have been integrated into the LFC framework of PSs to address these challenges, and Table 1 outlines the benefits and drawbacks associated with each technique.

The construction of the LFC system connected to the PS has employed a variety of control techniques (single-area and multi-area), each with pros and cons. A control strategy that can endure these difficulties and preserve the frequency stability associated with the multi-area PS must be developed, since the LFC system in the PS needs to be resilient to significant disruptions and significant uncertainties pertaining to the system parameters. Adaptive FFOPID control has been applied in the LFC system structure in this research to address uncertainties and disturbances while improving frequency stability in the TAPS. Additionally, reinforcement learning has been used to enhance the adaptive FFOPID controller's performance. For a number of important reasons, RL design has been used to enhance the fuzzy FOPID controller's performance in the two-area PS:

Automatic parameter optimization: RL allows the FFOPID controller to automatically adjust control parameters based on feedback received from the system. This automatic optimization process enables the controller to respond quickly and effectively to dynamic changes in the system. This feature is especially important in situations where system parameters are affected by disturbances or environmental changes. Using RL algorithms, the controller can use past experiences to better adjust parameters in the future, Consequently, the system's overall performance is improved.

- Uncertainty and disturbance management: RL increases the ability to manage uncertainties and disturbances. By finding patterns in the input and output data, the controller may use this technique to more accurately forecast how the system will behave. These predictions help the controller make better decisions when faced with unexpected conditions and prevent large fluctuations or errors. RL can also help the controller adapt to drastic changes in environmental conditions or system parameters.

- Performance-based reward: The controller in RL receives rewards according to how well it performs, and these incentives serve as inputs for improved learning. The FFOPID controller can determine and strengthen the most effective control tactics thanks to this incentive system. The controller's performance will thus gradually increase as a result of this learning process. This method also makes it possible to adjust to changing circumstances more quickly.
- Environmental change adaptation: The RL-influenced FFOPID controller is able to adapt to environmental changes with success. This adaptation is the outcome of the controller's rapid learning and condition adaption. For instance, in order to retain the intended performance, the controller can adjust its settings by evaluating fresh data and drawing on prior experiences in the event that the loading circumstances or system dynamics change. This feature improves the system's stability and dependability in the face of environmental changes.

The effectiveness of the suggested control method (FFOPID-RL) against disturbances and uncertainty of the two-area PS's parameters in various scenarios has been compared with that of the FFOPID, PDSMC, and SMC control methods. The findings indicate that the control method is better at lowering frequency deviations' settling times, lowering frequency deviations, and improving the dampening of oscillations in frequency related to with the two-area PS. The paper has several sections. In the second section, the TAPS and its state space equations are discussed. In the third section, the design of an improved FFOPID controller with a RL algorithm for the TAPS is discussed. In the fourth section, the proposed method (FFOPID-RL) is compared with other control methods in the TAPS. In the fifth section, the conclusion is also stated.

2. TAPS

Fig. 1 illustrates the TAPS dynamic model [27-30]. For frequency stability analysis, the first-order model of the TAPS components is used for a number of reasons, such as its ease of use and effectiveness in examining the PS's dynamic behavior, its capacity to forecast dynamic behavior, its responsiveness to minor disturbances, and its optimal analysis of dynamic stability [27-30]. A generator, a non-reheat turbine, and a governor are included in each section of this system [30]. A governor dead band (GDB) is taken into account in the governor model, and a generation rate constraint (GRC) is taken into account in the non-reheat turbine model [29,30].

Table 1. Outlines the benefits and drawbacks associated with each technique.

Deficiency of the method used	Lower frequency deviations	increase the PS's stability	robust to mild uncertainty	robust to extreme uncertainty	robust to mild disturbances	robust to severe disturbances
MPC Controller [12-14]	✓	✓	✓	×	×	×
SMC controller [15,16]	✓	✓	✓	✓	×	×
SMC Controller- meta-heuristic algorithm [17]	✓	✓	✓	✓	×	×
PID-LOA Controller [18]	✓	✓	✓	✓	×	×
PID-PSO Controller [19,20]	✓	✓	✓	✓	×	×
H_∞ Controller [21]	✓	✓	✓	✓	✓	×
Cascaded PD-PI Controller [22]	✓	✓	✓	✓	✓	×
Cascaded PDN-PI Controller [23]	✓	✓	✓	✓	×	×
FOPID-HGSO Controller [24]	✓	✓	✓	✓	×	×
FOPID-OSA Controller [25]	✓	✓	✓	×	✓	×
FOPID-FPA Controller [26]	✓	✓	✓	×	✓	×
Fuzzy Controller [27,28]	✓	✓	✓	×	✓	×
Fuzzy PID controller [29]	✓	✓	✓	×	✓	×
PDSMC Controller [30]	✓	✓	✓	✓	✓	×

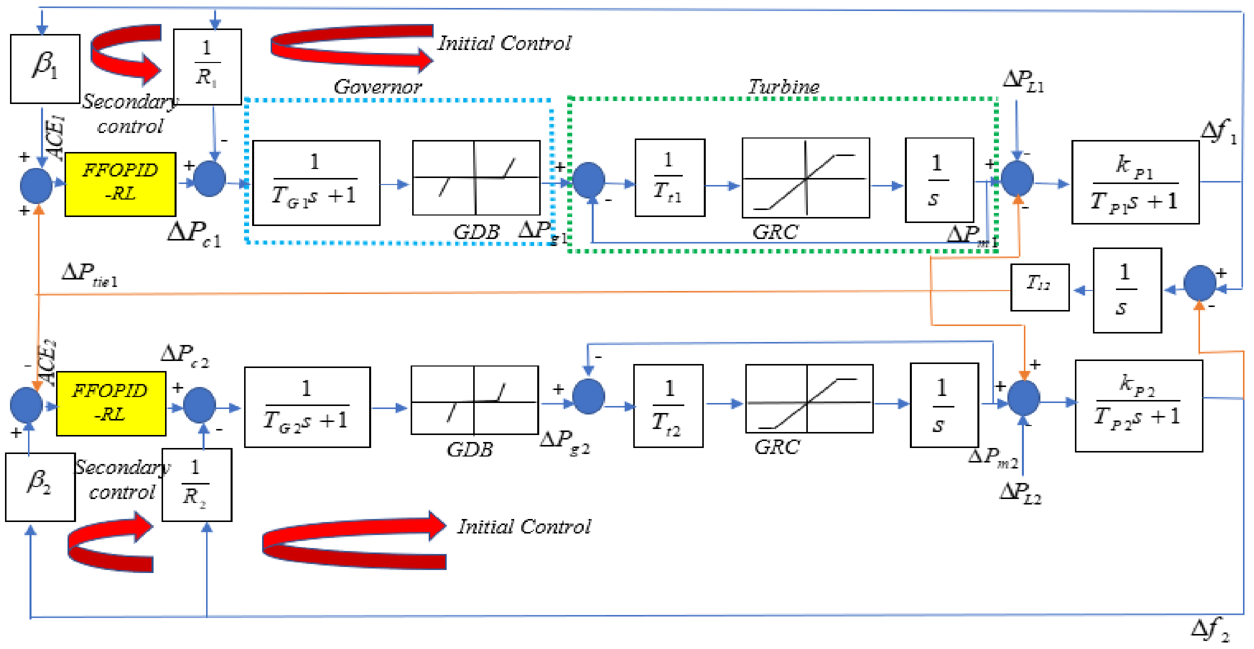

Fig. 1. TAPS dynamic model [27-30].

Equation (1) defines the governor-related transfer function [29,30].

$$G_H(s) = \frac{1}{T_{Gi}s+1}, \qquad i = 1,2 \qquad (1)$$

In Equation (1), T_{Gi} represents the governor's time constant for region i within the PS, where i can be area (1) or area (2) (i=1,2). Equation (2) displays the non-reheat turbine's transfer function [29,30].

$$G_T(s) = \frac{1}{T_{ti}s+1}, \qquad i = 1,2 \qquad (2)$$

In Equation (2), T_{ti} is the time constant of the non-reheat turbine corresponding to area i of the PS (i=1,2). In Equation (3), the transfer function corresponding to the generator is shown [29,30].

$$G_P(s) = \frac{k_{Pi}}{T_{Pi}s+1} \qquad (3)$$

In Equation (3), k_{pi} and T_{pi} are the gain and time constant of the PS of area i (i=1,2), respectively [29,30]. In Equation (4), the deviations of the communication error power are shown [30].

$$\Delta P_{tie_{ij}} = 2\pi T_{ij}\left(\int_0^t \Delta f_i dt - \int_0^t \Delta f_j dt\right) \qquad (4)$$

In Equation (4), T_{ij} is the coefficient of the connection line between the two PSs. In Equation (5), the area control error (ACE) corresponding to areas (1) and (2) is shown [30].

$$ACE_i = \sum_{i=1,2,i\neq n} \Delta P_{tie_{in}} + \beta_i \Delta f_i \qquad (5)$$

Equation (5) uses β to represent the PS's frequency bias and ACE to represent the area control error [29]. For each area of the PS, the state-space equation of the PS of area (1) and area (2) is derived using Equations (1) through (5), and it is shown using Equations (6) and (7) [27-30].

$$\begin{aligned} \dot{x} &= Ax(t) + Bu(t) + Dd(t) \\ y &= Cx(t) \end{aligned} \qquad (6)$$

$$\begin{bmatrix} \Delta\dot{P}_{gi} \\ \Delta\dot{P}_{mi} \\ \Delta\dot{f}_i \\ \Delta\dot{P}_{tie,i} \end{bmatrix} = \begin{bmatrix} \frac{-1}{T_{gi}} & 0 & \frac{-1}{R_iT_{gi}} & 0 \\ \frac{1}{T_{ti}} & -\frac{1}{T_{ti}} & 0 & 0 \\ 0 & \frac{k_{Pi}}{T_{Pi}} & \frac{-1}{T_{Pi}} & -\frac{k_{Pi}}{T_{Pi}} \\ 0 & 0 & 2\pi\sum\limits_{\substack{j=1 \\ j\neq i}} T_{ij}\Delta f & 0 \end{bmatrix} \begin{bmatrix} \Delta P_{gi} \\ \Delta P_{mi} \\ \Delta f_i \\ \Delta P_{tie,i} \end{bmatrix} + \begin{bmatrix} \frac{1}{T_{gi}} \\ 0 \\ 0 \\ 0 \end{bmatrix} [\Delta P_{ci}] + \begin{bmatrix} 0 & 0 \\ 0 & 0 \\ -\frac{k_{Pi}}{T_{Pi}} & 0 \\ 0 & -2\pi \end{bmatrix} \begin{bmatrix} \Delta P_{Li} \\ \Delta v_i \end{bmatrix}$$

$$y = ACE = \begin{bmatrix} 0 & 0 & \beta_i & 1 \end{bmatrix} \begin{bmatrix} \Delta P_{gi} \\ \Delta P_{mi} \\ \Delta f_i \\ \Delta P_{tie,i} \end{bmatrix} \qquad (7)$$

A is the system matrix, B is the system input vector, u(t) is the control input, D is the disturbance vector, d(t) is the external disturbance that impacts the system, and x(t) is the state vector in Equation (6). In Equation (7), ΔP_{Gi} represents the area i generator output power variation, ΔP_{mi} represents the area i mechanical power variation, Δf_i represents the area i frequency deviation, ΔP_{Li} represents the load variation, ΔP_{ci} represents the area i control signal, ΔP_{tie} represents the output power of the communication line between the two areas, and Δv_i This signal corresponds to the interchange control command linking area 1 and area 2 within the power network.

3. Design of an improved Fuzzy FOPID controller with RL for the ‹TAPS

3-1. FOPID Controller

3-1-1. Definition and characteristics of FOPID controller

FOPID is an advanced version of the classical PID controller in which the derivative and integration are performed with fractional orders [31-33]. This type of controller has several advantages over the PID controller, including greater flexibility, more accurate control, better transient response, reduced steady-state error, and better compatibility with optimization algorithms and neural networks [31-33].

Due to these features, the use of FOPID controller can have better performance in complex dynamic systems.

The FOPID controller signal is obtained from Equation (8) [34-36].

$$u(t) = K_p e(t) + K_i D_t^{-\alpha} e(t) + K_d D_t^{\beta} e(t) \tag{8}$$

The proportional coefficient in Equation (8) is denoted by K_p, the integral by K_i, the derivative by K_d, the fractional integration operator of order α by $D_t^{-\alpha}$, the fractional differentiation operator of order β by D_t^{β}, and the control error by e(t).

3-1-2. Definition of fractional derivative and fractional integration in FOPID controller

For the FOPID controller, fractional-order derivative and integration are a generalization of the ordinary derivative and integration operations and are defined as Equation (9) [34-36].

$$D_t^{\nu} f(t) = \frac{1}{\Gamma(n-\nu)} \frac{d^n}{dt^n} \int_0^t (t-\tau)^{n-\nu-1} f(\tau) d\tau \tag{9}$$

In Eequation (9), Γ is the gamma function, ν is the fractional order, which can be a fractional value or even negative, and n is the smallest integer greater than ν.

3-2. FFOPID Controller

3-2-1. Advantages of FFOPID Controller

The FFOPID controller has several advantages over the conventional FOPID controller, including [31-33]:

- Automatic parameter tuning: In the FOPID controller, the control parameters are controlled online based on fuzzy rules, which improves the control performance against dynamic changes in the system
- Improvement against system uncertainties: This controller is robust against system uncertainties and manages them.
- Accurate and fast response: This controller provides a fast and accurate response to input changes and reduces the settling time and also reduces the stable error.
- Greater flexibility: This feature of the fuzzy FOPID controller allows for more complex and better design for the systems.
- Considering the features mentioned above, in this paper, the FFOPID controller has been used to improve the performance of the LFC system in a TAPS.

3-2-2. Fuzzy structure and system related to the FFOPID controller

Fig. 2. depicts the structure of a fuzzy system [37]. A defuzzifier, a rule base, an inference engine, and a fuzzifier are the primary parts of this system [37]. The fuzzifier section's job is to turn numerical and exact inputs into fuzzy data [37]. Incorporating a series of fuzzy rules in the "if...then" format is the responsibility of the rule base section [38]. These guidelines establish what the output should be under various input circumstances and are created using the designers' expertise or knowledge [37,38]. The task of the inference engine is to evaluate the degree of compliance of the fuzzy inputs with the rules in the rule base, and based on this compliance, various decisions will be produced that indicate possible outputs for the system [37,38]. In the defuzzifier, the results obtained from the inference engine, which are in the form of fuzzy sets, will be converted into precise and numerical values [37,38]. This process helps in choosing the best decision based on the outputs [37,38].

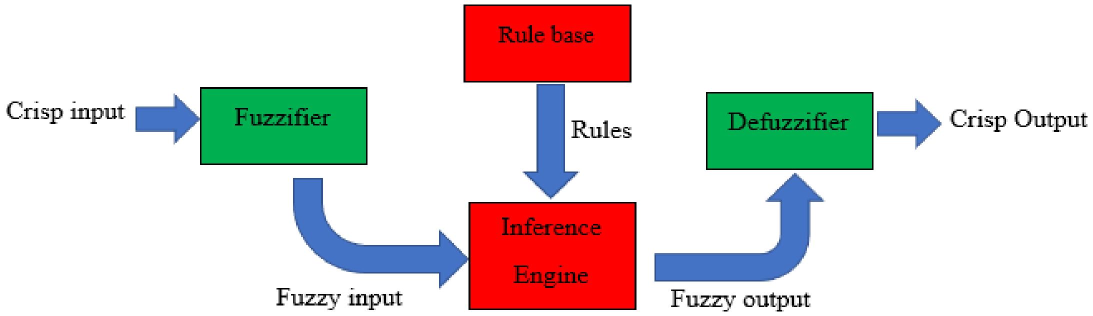

Fig. 2. The structure of a fuzzy system [37].

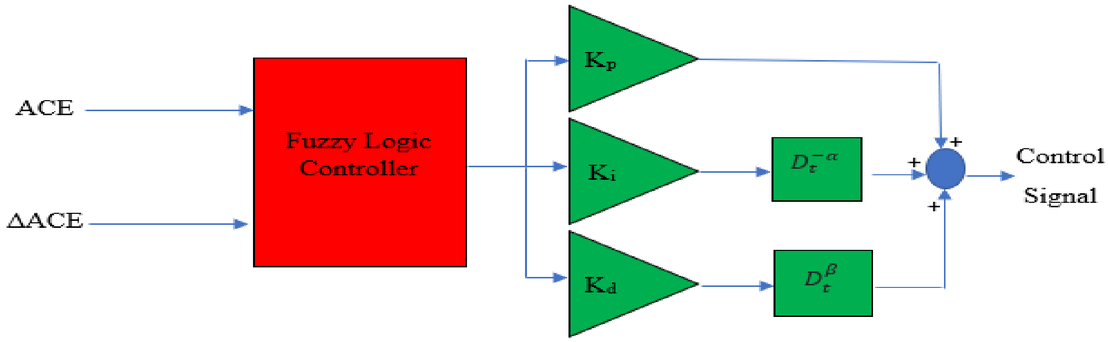

Fig. 3. Input and output variables for the FFOPID controller.

In this paper, a fuzzy system is used to adjust the parameters Kp, Ki, Kd, α, and β of the FOPID controller.

Table 2. The fuzzy inference rules for K_p.

$ACE = e(t)$	$\Delta ACE = \dot{e}(t)$						
	NB	NM	NL	Z	PL	PM	PB
NB	PB	PM	PL	PL	PM	PM	PB
NM	PM	PL	PL	PL	Z	PM	PB
NL	PL	PL	Z	Z	Z	PL	PM
Z	PL	PL	Z	Z	Z	PL	PL
PL	Z	Z	Z	Z	Z	Z	PL
PM	Z	PL	PL	PL	PM	PM	PB
PB	PB	PM	PM	PM	PM	PB	PB

3-3. Implementation of the fuzzy FOPID controller of the LFC structure related to the two-area PS

The implementation of the FFOPID controller of the LFC structure related to the TAPS consists of several steps.

3-3-1. Definition of input and output variables for the FFOPID controller

This work makes use of the Mamdani fuzzy inference system. The input and output variables for the FFOPID controller are displayed in Fig. 3. This fuzzy system's inputs are the ACE and the ΔACE, and its outputs are, in that order, K_p, K_i, K_d, α, and β.

3-3-2. Define membership functions for the FFOPID controller's input and output variables

Membership functions for inputs and outputs are divided into seven categories, NB, NM, NL, Z, PL, PM and PB in order to classify variables into linguistic values. In Fig. 4, membership functions for inputs and outputs of FFOPID are defined.

3-3-3. Definition of fuzzy inference rules for determining input variables related to the FFOPID controller

Fuzzy inference rules are taken into consideration in order to ascertain the output values of the FFOPID controller. The fuzzy inference rules for K_p are based on ACE and ΔACE, as shown in Table 2. The fuzzy inference rules for K_i are based on ACE and ΔACE, as shown in Table 3. The fuzzy inference rules for K_d are based on ACE and ΔACE, as shown in Table 4. The fuzzy inference criteria for α, β are based on ACE and ΔACE, as shown in Table 5.

Table 3. The fuzzy inference rules for K_i.

$ACE = e(t)$	$\Delta ACE = \dot{e}(t)$						
	NB	NM	NL	Z	PL	PM	PB
NB	PB	PB	PM	PM	PL	PL	Z
NM	PM	PM	PL	PL	Z	Z	NL
NL	PM	PL	PL	Z	Z	NL	NM
Z	PL	PL	Z	Z	Z	NL	NM
PL	PL	Z	Z	Z	Z	NL	NM
PM	Z	Z	NL	NL	NM	NM	NB
PB	Z	NL	NM	NM	NM	NB	NB

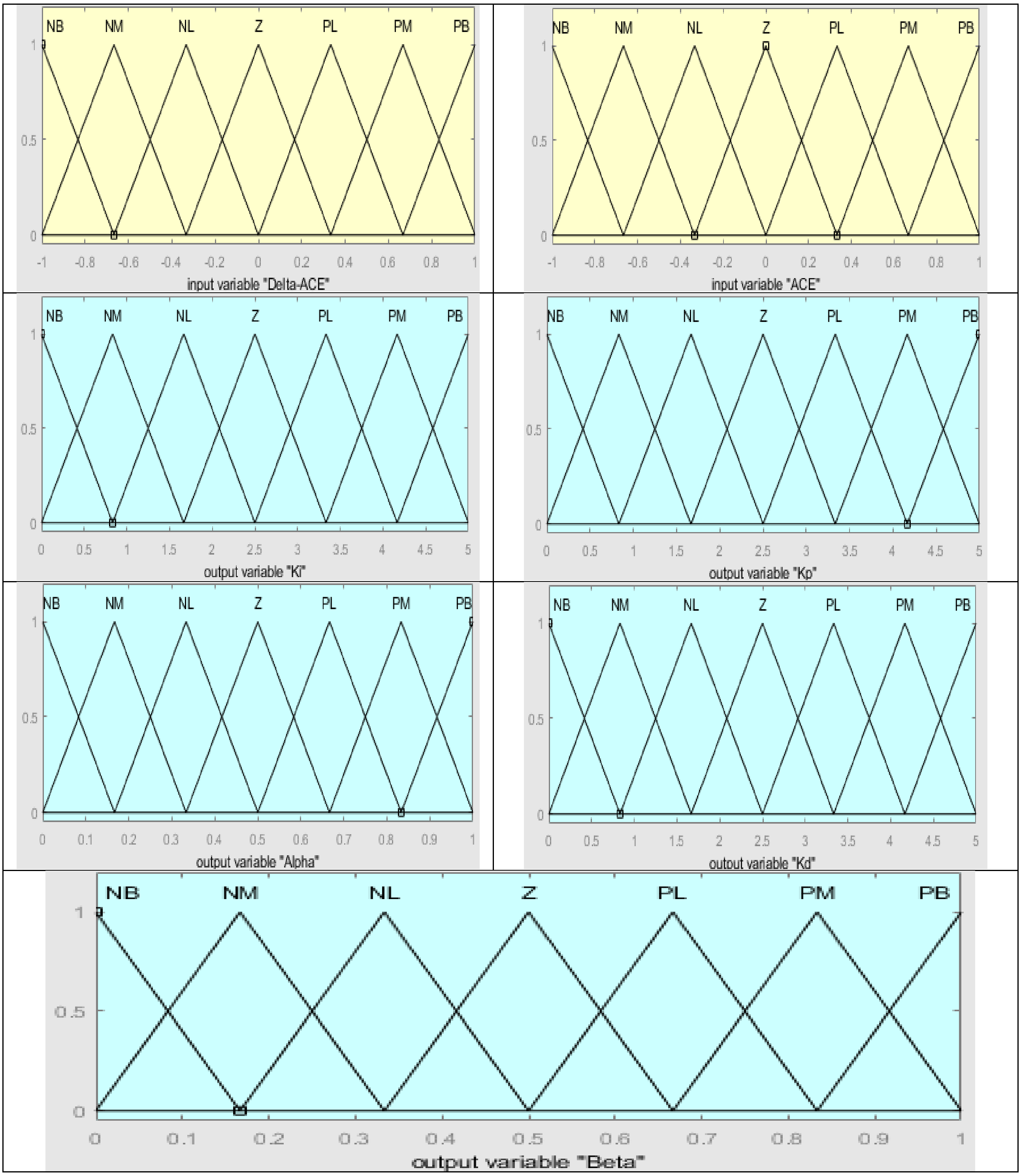

Fig. 4. The membership functions for inputs and outputs of fuzzy FOPID.

Table 4. Fuzzy inference rules for K_d.

$ACE = e(t)$	$\Delta ACE = \dot{e}(t)$						
	NB	NM	NL	Z	PL	PM	PB
NB	PB	PM	PL	Z	Z	NL	NM
NM	PM	PL	PL	Z	Z	NL	NM
NL	PL	PL	Z	Z	NL	NM	NB
Z	PL	Z	Z	Z	Z	Z	PL
PL	Z	Z	Z	Z	Z	Z	PL
PM	Z	Z	PL	PL	PM	PM	PB
PB	Z	PL	PM	PM	PM	PB	PB

Table 5. The fuzzy inference rules for α, β.

$ACE = e(t)$	$\Delta ACE = \dot{e}(t)$						
	NB	NM	NL	Z	PL	PM	PB
NB	PB	PM	PL	Z	Z	NL	NM
NM	PM	PL	Z	Z	Z	NL	NM
NL	PL	PL	Z	Z	Z	NL	NM
Z	PL	Z	Z	Z	Z	Z	PL
PL	Z	Z	Z	Z	Z	Z	PL
PM	Z	Z	PL	PL	PM	PM	PB
PB	Z	PL	PM	PM	PM	PB	PB

4-3-3. Defuzzification of variables related to the FFOPID controller

The centroid approach uses the output membership function's center of gravity to produce the final output, which contains the FOPID controller coefficients. In this study, we derive the formula for defuzzification of the fuzzy system using the center of gravity approach from Equation (10) [37, 38].

$$Output = \frac{\sum_i \mu_i x_i}{\sum_i \mu_i} \quad (10)$$

In Equation (10), Output is the final de-fuzzified output (Kp, Ki, Kd, α and β), i represents each output language set, μ_i is the calculated membership degree for the ith output language set, and x_i is the center or representative value of the ith output language set (the center of each triangular membership function is considered).

In this paper, RL is used to improve the performance of a FFOPID controller in a TAPS for several key reasons:

1) Automatic parameter optimization 2) Uncertainty and disturbance management 3) Performance-based reward 4) Adaptation to environmental changes.

4-4. RL

Q-learning is a popular algorithm in RL that has many advantages that make it suitable for various applications [39]. The following are the key reasons why Q-learning is suitable: Overall, the model-free nature, simplicity, flexibility, effective exploration strategies, and convergence properties of Q-learning make it a powerful choice for RL applications in various domains [40]. The ability to learn optimal policies without requiring a detailed understanding of the environment increases its applicability in real-world scenarios where such details may not be available [40-42].

A value-based RL technique called Q-Learning seeks to determine the appropriate course of action for an agent in every circumstance so that it can maximize its long-term reward [40-42]. The fundamental ideas of the Q-Learning algorithm are as follows:

- State: The current state of the agent in the environment, denoted by s.
- Action: An action that the agent can take, denoted by a.
- Reward: The feedback that the agent receives after performing each action, indicating whether that action is positive or negative. This is denoted by r.
- Policy: A map that suggests the optimal action for each situation.
- Q-Value: The anticipated benefit that the agent will get for carrying out action a in state s and thereafter adhering to the best course of action.

Finding the optimal value function Q*(s, a), or an estimate of the total expected reward that the agent obtains from state s by carrying out action a and then adhering to the optimal policy, is the aim of Q-Learning. Equation (11) illustrates the use of a recurrence relation known as the Bellman equation to derive this function [40-42].

$$Q^*(s,a) = E[r + \gamma \max_{\alpha'} Q(s',a')|s,a] \quad (11)$$

s stands for the present state, a for the current action, r for the instant reward for doing action an in state s, and s' for the new state that is the consequence of executing action a, the next action to be performed in state s' by a', and the discount factor γ, which ranges from 0 to 1, that establishes the significance of future rewards [40].

Equation (12) states that the Q-Learning update rule is used at each step to update the value of Q(s, a) for the current state and action [41,42]:

$$Q(s,a) \leftarrow Q(s,a) + \delta[r + \gamma \max_{\alpha'} Q(s',a') - Q(s,a)] \quad (12)$$

In Equation (12), δ is the learning rate that determines the importance of new experiences (a number between 0 and 1).

Equation (12) means that the current value of Q(s, a) is combined with a new value calculated from the received reward r and the maximum value of Q for the new state s'. This updating process causes the estimate of Q(s,a) to gradually approach the optimal value Q*(s,a). The steps of the Q-Learning algorithm are as follows [41,42].

1) Initialization: First, the values of Q(s,a) for all states and actions are initialized to a fixed value (such as zero).

2) Learning loop:

For each step:

2-1) Observe the current state s.

2-2) Select an action a using a policy such as greedy-ε:

2-3) Policy greedy-ε: For exploration, choose a random action with probability ε. For exploitation, choose the optimal action with probability 1-ε.

2-4) Get reward r and new state s' by carrying out action a.

2-5) Utilizing the update rule Q, refresh the value of Q(s, a).

2-6) Change the state to s'.

3) Stopping condition: The learning loop continues until it reaches a stopping condition (such as a certain number of steps or episodes, or the convergence of $Q(s,a)$ to a stable value). In Fig. 5, the structure of the RL algorithm is shown [40-42]. In order to optimize the settings of a FFOPID controller for the two-area PS, RL is crucial in this work. In order to improve the frequency stability and performance of the LFC system, RL aims to lower the errors (ACE) in each section of the PS in response to uncertainties and disturbances. Each episode of the RL process corresponds to a cycle of contact with the environment (two-area PS). After every action, the agent is rewarded according on how well it performed. In this method, the reward is calculated as the negative of the absolute value of the ACE of each area of the PS, which encourages the reduction of ACE values. Also, in this method, the agent uses the feedback of previous actions (ACE values and control signals) to update its understanding of how to effectively adjust the control parameters.

The RL inputs in this paper are:1) ACE (2) ΔACE- Input range: [-1, 1] (normalized).
The outputs of the fuzzy inference system (FIS) that are tuned through RL are:
1) K_p 2) K_i 3) K_d, 4) α, 5) β

This adaptive approach allows for better handling of uncertainties and disturbances in a dynamic environment such as a PS.

4-5. Steps to design an improved FFOPID controller with RL algorithm for a TAPS

The steps for designing an improved FFOPID controller with RL algorithm for a TAPS are given below:
Step 1: Start
Step 2: Define Nominal Parameters
Step 3: Introduce Uncertainty to PS parameters
Step 4: Define Disturbance Function
Step 5: Set Up Fuzzy FOPID Controller
Step 6: Define State-Space Model Matrices
Step 7: Initialize State Vectors
.Step 8: RL Loop
Step 9: Plotting Results
The pseudocode for designing an improved FFOPID controller with RL algorithm for a two-area PS is given below:

```
//Step 1:
Start
// Step 2: Define nominal parameters for the TAPS
Define nominal parameters R1, kp1, Tp1, TG1, β1 , Tt1 for area1
Define nominal parameters R2, kp2, Tp2, TG2, β2 , Tt2 for Area 2
Define nominal tie-line power transfer coefficient Tij _nominal
// Step 3: Introduce uncertainty to parameters
Set uncertainty_level to 0.2 (20% uncertainty)
Generate random values for R1, kp1, Tp1, TG1, β1 , Tt1 , R2, kp2, Tp2, TG2, β2 , Tt2 using the uncertainty level
// Step 4: Define disturbance function
Define disturbance function as a sine wave disturbance
// Step 5: Set up fuzzy FOPID controller settings
Create fuzzy inference system (FIS) named 'Fuzzy_FOPID_Controller'
Add inputs ACE and Delta_ACE to the FIS
Define membership functions for ACE and Delta_ACE
Define output membership functions for Kp, Ki, Kd, Alpha, Beta
// Step 6: Define state-space model matrices for Area 1 and Area 2
Define state-space model matrices A1 and B1_state for Area 1
Define state-space model matrices A2 and B2_state for Area 2
// Step 7: Initialize state vectors for both areas
Set initial states x_state_1 and x_state_2 to zero vectors
// Step 8: Set up reinforcement learning loop over specified episodes
For each episode from 1 to num_episodes do:
   // Step 8a: Calculate disturbance value for this step
   disturbance_value = disturbance(episode)
   // Step 8b: Calculate ACE and Delta_ACE for each area
   ACE_1 = Generate random value between -0.5 and +0.5 plus disturbance_value
   Delta_ACE_1 = ACE_1 - previous state value of x_state_1(1)
   ACE_2 = Generate random value between -0.5 and +0.5 plus disturbance_value
   Delta_ACE_2 = ACE_2 - previous state value of x_state_2(1)
   // Step 8c: Apply fuzzy controller to get outputs for both areas
   // Step 8d: Extract control parameters from fuzzy outputs
   Kp_1 = output_1(4)
   Ki_1 = output_1(5)
   Kd_1 = output_1(6)
```

```
    Alpha_1= output_1(7)
…Beta_1= output_1(8)
    Kp_2 = output_2(4)
    Ki_2 = output_2(5)
    Kd_2 = output_2(6)
    Alpha_2= output_2(7)
…Beta_2= output_2(8)
    // Step 8e: Calculate control signals using
FOPID control formula
    u_1 = Calculate control signal for Area 1
using Kp_1, Ki_1, Kd_1, Alpha_1, Beta_1
    u_2 = Calculate control signal for Area 2
using Kp_2, Ki_2, Kd_2, Alpha_2, Beta_2
    // Step 8f: Update states for both areas using
state-space model equations
    x_state_1 = A1 * x_state_1 + B1_state * u_1
    x_state_2 = A2 * x_state_2 + B2_state * u_2
    // Step 8g: Record frequency changes in each
area based on updated states
    frequency_changes_1[episode] =
x_state_1(1)
    frequency_changes_2[episode] =
x_state_2(1)
End For
```

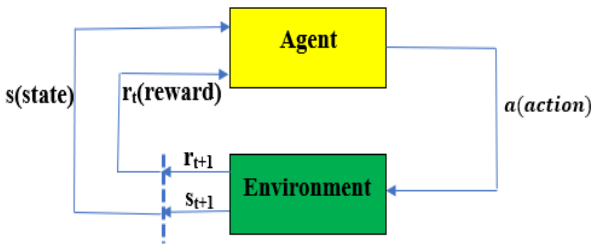

Fig. 5. The structure of the RL algorithm [40-42].

4. Simulation

The parameters of the system under study are displayed in Table 6. To compare the performance of the suggested approach (FFOPID-RL) with the control methods FFOPID, PDSMC, and SMC in the LFC structure of the TAPS, four scenarios are taken into consideration in this work. The suggested technique (FFOPID-RL) is contrasted with other control strategies (FFOPID, PDSMC, and SMC) in scenario (1) to guard against significant disruptions that enter the TAPS. In scenario (2), the proposed method is compared against alternative control strategies to safeguard the TAPS from small disturbances. In scenario (3), the proposed method is combined with additional control strategies FFOPID, PDSMC, and SMC to analyze the simultaneous effects of severe disturbances and mild uncertainty in the power system parameters. In order to evaluate how well the suggested approach performs in the face of significant disruptions and extreme uncertainty about the PS characteristics, scenario (4) is also taken into consideration.

Table 6. The parameters of the system under study.

Parameters	Area (1)	Area (2)
k_{pi}	120 Hz/pu. MW	115 Hz/pu. MW
T_{pi}	20s	20s
T_{Gi}	0.08s	0.06s
T_{ti}	0.40s	0.44s
β	0.3483pu/Hz	0.3827pu/HZ
Tij	0.20 pu/Hz	0.20 pu/Hz
R	3Hz/pu	2.73Hz/pu

4-1. Scenario (1)

Fig. 6 displays the load disturbances on area (1) of the PS. Fig. 7 illustrates the load disturbances on area (2) of the PS. Based on the FFOPID-RL, FFOPID, PDSMC, and SMC control techniques, the frequency response of area (1) and area (2) of the PS is displayed in Figs. 8 and 9 correspondingly. As demonstrated in Figs. 8 and 9, the proposed FFOPID-RL controller surpasses other control methods in performance and remains robust against large load disturbances affecting areas 1 and 2 of the PS. Moreover, the proposed technique achieves a faster settling time and effectively reduces frequency deviations in areas 1 and 2 of the power system. Table 7 presents the performance results of the various controllers employed in the load-frequency control configuration for scenario 1.

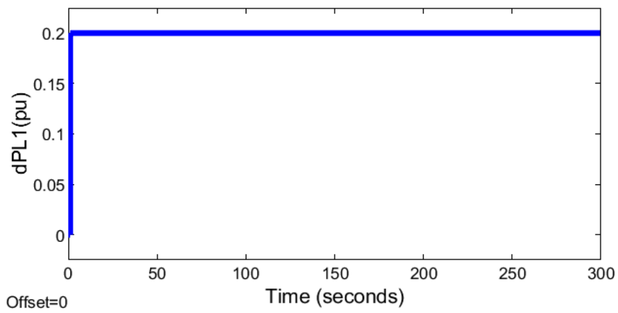

Fig. 6. The load disturbances affecting the area (1) of the PS, Scenario (1) [25].

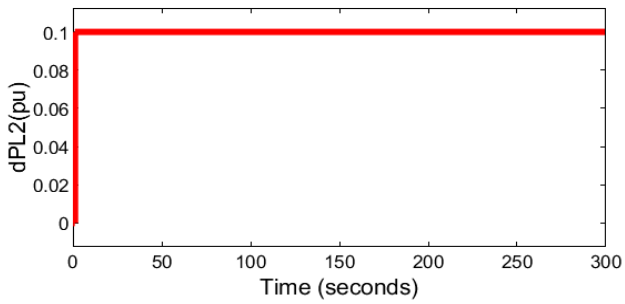

Fig. 7. The load disturbances affecting the area (2) of the PS, Scenario (1) [25].

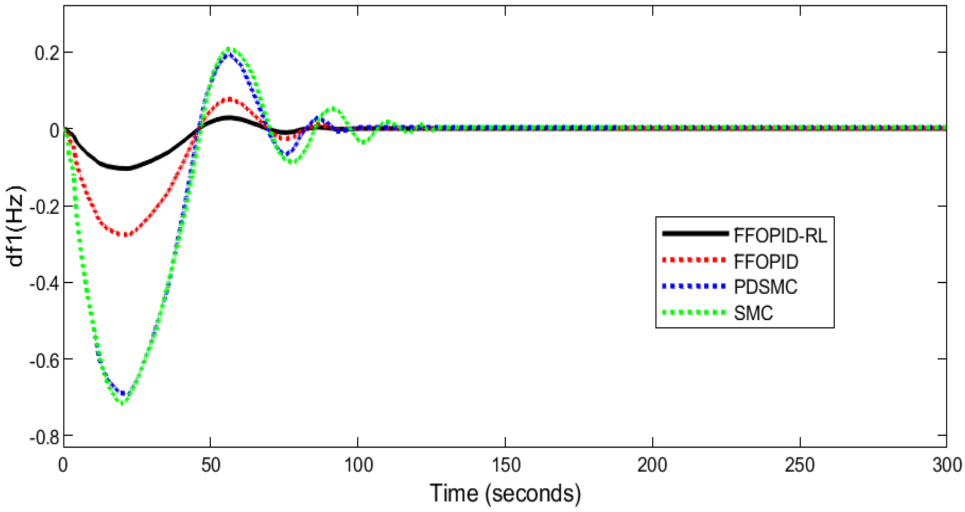

Fig. 8. The frequency response of area (1) of the PS, Scenario (1).

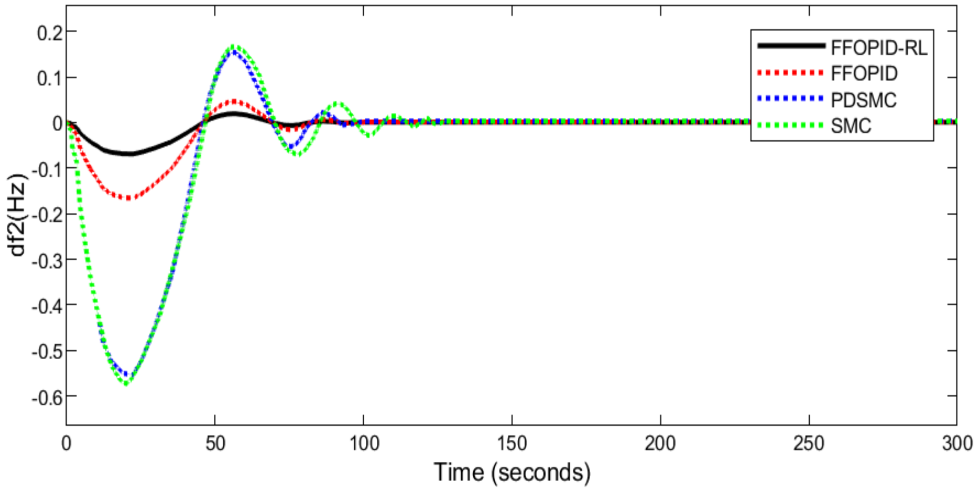

Fig. 9. The frequency response of area (2) of the PS, Scenario (1).

Table 7. Results of different controllers used in the LFC structure related to scenario (1).

Controller	Δf_1(Hz)			Δf_2(Hz)		
	MO (Hz)	MU (Hz)	ST (sec)	MO (Hz)	MU (Hz)	ST (sec)
FFOPID-RL	0.05	0.11	73	0.04	0.09	71
FFOPID	0.08	0.28	81	0.07	0.14	79
PDSMC	0.19	0.70	84	0.16	0.56	82
SMC	0.20	0.70	120	0.14	0.54	120

4-2. Scenario (2)

Fig. 10, which depicts the load disturbances on area (1) of the PS. Fig. 11 illustrates the load disturbances on area (2) of the PS. Based on the FFOPID-RL, FFOPID, PDSMC, and SMC control techniques, the frequency response of area (1) and area (2) of the PS is depicted in Figs. 12 and 13 correspondingly. As illustrated in Figs. 12 and 13, the proposed FFOPID-RL controller surpasses other control techniques and remains robust against small load disturbances affecting areas 1 and 2 of the PS. Furthermore, the proposed method exhibits a faster settling time and effectively diminishes the frequency deviations in areas 1 and 2 of the PS. Table 8 displays the outcomes of the various controllers employed in the LFC structure associated with scenario (2).

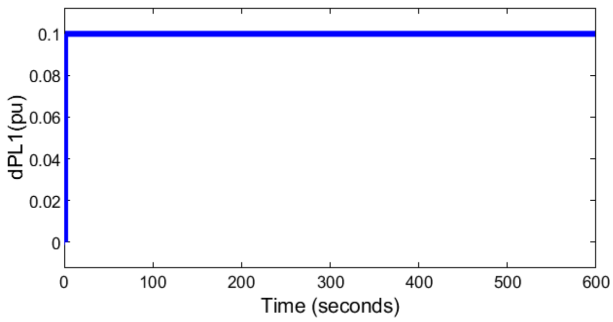

Fig. 10. The load disturbances affecting the area (1) of the PS, Scenario (2) [25].

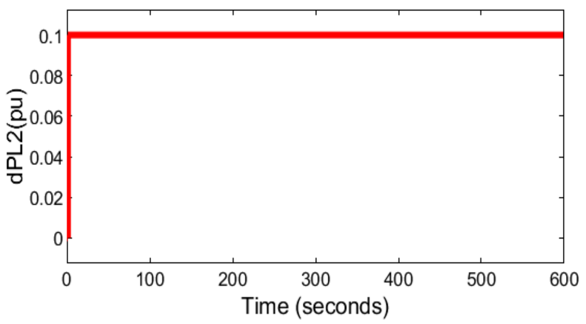

Fig. 11. The load disturbances affecting the area (2) of the PS, Scenario (2) [25].

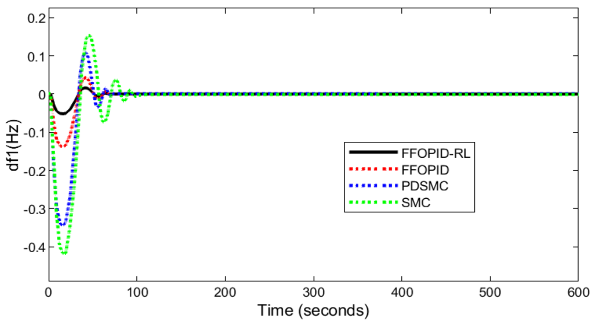

Fig. 12. The frequency response of area (1) of the PS, Scenario (2).

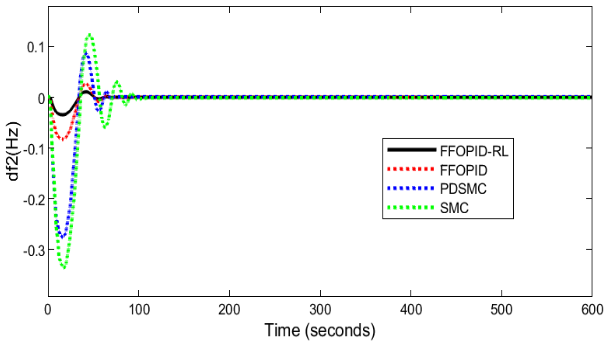

Fig. 13. The frequency response of area (2) of the PS, Scenario (2).

Table 8. Results of different controllers used in the LFC structure related to scenario (2).

Controller	Δf_1(Hz)			Δf_2(Hz)		
	MO (Hz)	MU (Hz)	ST (sec)	MO (Hz)	MU (Hz)	ST (sec)
FFOPID-RL	0.03	0.06	72	0.03	0.09	71
FFOPID	0.04	0.14	80	0.07	0.14	79
PDSMC	0.10	0.35	81	0.08	0.28	80
SMC	0.11	0.43	112	0.15	0.35	113

4-3. Scenario (3)

Fig. 6 illustrates the load disturbances associated with the PS that enter area (1). Fig. 7 illustrates the load disturbances associated with the PS that enter area (2) (T_{G1}=T_{G2}=+20%). The frequency response of areas (1) and (2) associated with the PS is depicted in Figs. 14 and 15, respectively, using the FFOPID-RL, FFOPID, PDSMC, and SMC control techniques. The suggested controller (FFOPID-RL), as shown in Figs. 14 and 15, has outperformed alternative control strategies and is resilient to significant load disruptions and uncertainty pertaining to the PS's characteristics. Moreover, the proposed method achieves quicker stabilization and effectively reduces frequency fluctuations in areas 1 and 2 of the PS. Table 9 displays the outcomes of the various controllers employed in the LFC structure associated with scenario (3).

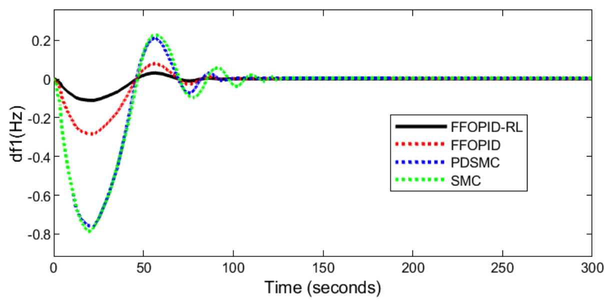

Fig. 14. The frequency response of area (2) of the PS, Scenario (3).

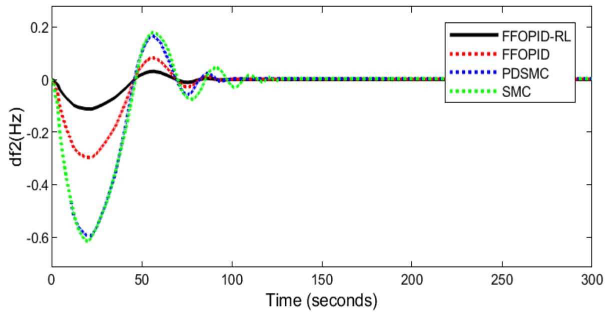

Fig. 15. The frequency response of area (2) of the PS, Scenario (3).

Table 9. Results of different controllers used in the LFC structure related to scenario (3).

Controller	Δf_1(Hz)			Δf_2(Hz)		
	MO (Hz)	MU (Hz)	ST (sec)	MO (Hz)	MU (Hz)	ST (sec)
FFOPID-RL	0.051	0.12	73	0.05	0.10	72
FFOPID	0.09	0.30	82	0.07	0.26	81
PDSMC	0.21	0.77	88	0.20	0.59	89
SMC	0.22	0.78	133	0.21	0.61	135

4-4. Scenario (4)

Fig. 6 displays the load disturbances on area (1) of the PS (T_{G1}=T_{G2}=+30%, k_{p1}=k_{p2}=-%30). Fig. 7 illustrates the load disturbances on area (2) of PS. The frequency response of areas (1) and (2) of the PS based on the FFOPID-RL, FFOPID, PDSMC, and SMC control techniques is displayed in Figs.

16 and 17. The suggested controller (FFOPID-RL), as shown in Figs. 16 and 17, has outperformed alternative control strategies and is resilient to significant load disruptions and parameter uncertainty associated with the PS. Moreover, the proposed method achieves quicker stabilization and effectively reduces frequency fluctuations in areas 1 and 2 of the PS. The findings of several controllers utilized in the LFC structure linked to scenario (4) are provided in Table 10.

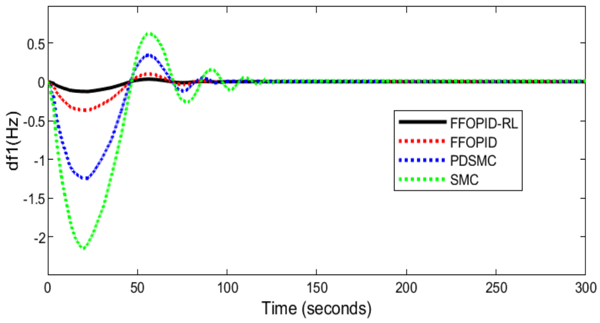

Fig. 16. The frequency response of area (1) of the PS, Scenario (4).

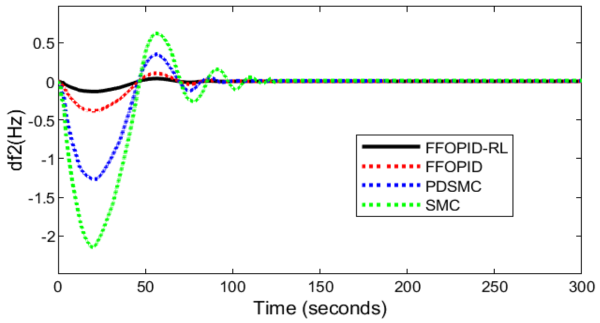

Fig. 17. The frequency response of area (2) of the PS, Scenario (4).

Table 10. Results of different controllers used in the LFC structure related to scenario (4).

Controller	Δf_1(Hz)			Δf_2(Hz)		
	MO (Hz)	MU (Hz)	ST (sec)	MO (Hz)	MU (Hz)	ST (sec)
FFOPID-RL	0.054	0.15	74	0.052	0.18	73
FFOPID	0.11	0.37	85	0.10	0.35	84
PDSMC	0.41	1.23	101	0.43	1.21	93
SMC	0.72	2.1	140	0.73	2.12	141

5. Conclusion

In this paper, in order to improve the frequency stability in a multi-area PS and to deal with disturbances and uncertainties, an adaptive FFOPID controller was designed in the LFC structure, and the performance of the adaptive FFOPID controller was improved using RL. According to the simulation results, RL has improved the performance of the adaptive FFOPID controller against disturbances and uncertainties of the TAPS, and also the control system has better adaptation to its surrounding environment. Also, the proposed method (FFOPID-RL) has been compared with different control methods such as FFOPID, PDSMC, and SMC, and the results show that the control method is superior in reducing the settling time of frequency deviations, reducing frequency deviations, and improving the damping of frequency oscillations related to the TAPS.

References

[1] Mishra, D. K., Mohanty, A., & Ray, P. K. (2024). An optimal frequency regulation in interconnected PS through differential evolution and firefly algorithm. Soft Computing, 28(1), 593-606.

[2] Goud, V., Goud, H., Salwan, C. et al. (2024) Metaheuristic algorithm based PID controller using MRAC techniques for control of a nonlinear system. Soft Computing. https://doi.org/10.1007/s00500-024-10360-7

[3] Amiri, F., & Moradi, M. H. (2023). Improvement of Frequency stability in the power system considering wind turbine and time delay. Journal of Renewable Energy and Environment, 10(1), 9-18.

[4] Jagatheesan, K., Boopathi, D., Samanta, S., Anand, B., & Dey, N. (2024). Grey wolf optimization algorithm-based PID controller for frequency stabilization of interconnected power generating system. Soft Computing, 28(6), 5057-5070.

[5] Amiri, F., Moradi, M. H., & Eskandari, M. (2024). Suppression of low-frequency oscillations in hybrid/multi microgrid systems with an improved model predictive controller. IET Renewable Power Generation, 18(9-10), 1691-1709.

[6] Qiao, S., Liu, X., Wang, D., & Ge, S. S. (2024). Security Concern and Fuzzy Output Sliding Mode Load Frequency Control of PSs. Information Sciences, 120793.

[7] Priyadarshani, S., & Subhashini, K. R. (2024). Search and Rescue Optimization Algorithm Tuned FOTID Controller for Load Frequency Control of PS. Iranian Journal of Science and Technology, Transactions of Electrical Engineering, 1-23.

[8] Ghafoor, R., Guanghua, L., Gulzar, M. M., Irfan, R., Alqahtani, M., & Khalid, M. (2024). Load frequency control of multi-area PS incorporated renewable energy considering electrical vehicle effect using modified cascaded controller tuned by BESSO algorithm. Heliyon.

[9] Zhang, J., Peng, F., Wang, L., Yang, Y., & Li, Y. (2024). A load frequency control strategy based on double deep Q-network and upper confidence bound algorithm of multi-area interconnected PSs. Computers and Electrical Engineering, 120,

109778.

[10] Ba Wazir, A., Althobiti, A., Alhussainy, A. A., Alghamdi, S., Vellingiri, M., Palaniswamy, T., & Rawa, M. (2024). A Comparative Study of Load Frequency Regulation for Multi-Area Interconnected Grids Using Integral Controller. Sustainability, 16(9), 3808.

[11] Jain, D., & Bhaskar, M. K. (2024). Optimization of controllers using soft computing technique for load frequency control of multi-area deregulated PS. International Journal of Applied, 13(1), 52-65.

[12] An, Z., Liu, X., Xiao, G., Song, G., & Wang, P. (2024). Tube-based MPC strategy for load frequency control of multi-area interconnected PS with HESS. *Journal of Energy Storage*, *99*, 113340.

[13] Liu, X., Wang, C., Kong, X., Zhang, Y., Wang, W., & Lee, K. Y. (2023). Tube-based distributed MPC for load frequency control of PS with high wind power penetration. *IEEE Transactions on PSs*, *39*(2), 3118-3129.

[14] Taher, A. M., Hasanien, H. M., Aleem, S. H. A., Tostado-Véliz, M., Ćalasan, M., Turky, R. A., & Jurado, F. (2023). Optimal model predictive control of energy storage devices for frequency stability of modern PSs. *Journal of Energy Storage*, *57*, 106310.

[15] Biswas, D. K., Debbarma, S., & Singh, P. P. (2024). LFC of multi-area PS using a robust full-order terminal sliding mode controller considering communication delay. *Electrical Engineering*, 1-15.

[16] Alhelou, H. H., Nagpal, N., Kassarwani, N., & Siano, P. (2023). Decentralized optimized integral sliding mode-based load frequency control for interconnected multi-area PSs. *IEEE Access*, *11*, 32296-32307.

[17] Tran, A. T., Duong, M. P., Pham, N. T., & Shim, J. W. (2024). Enhanced sliding mode controller design via meta-heuristic algorithm for robust and stable load frequency control in multi-area PSs. *IET Generation, Transmission & Distribution*, *18*(3), 460-478.

[18] Sharma, A., & Singh, N. (2024). Load frequency control of connected multi-area multi-source PSs using energy storage and lyrebird optimization algorithm tuned PID controller. *Journal of Energy Storage*, *100*, 113609.

[19] Ogar, V. N., Hussain, S., & Gamage, K. A. (2023). Load frequency control using the particle swarm optimisation algorithm and Pid controller for effective monitoring of transmission line. *Energies*, *16*(15), 5748.

[20] Dhanasekaran, B., Kaliannan, J., Baskaran, A., Dey, N., & Tavares, J. M. R. (2023). Load frequency control assessment of a PSO-PID controller for a standalone multi-source PS. *Technologies*, *11*(1), 22.

[21] Shen, H., Jiao, S., Park, J. H., & Sreeram, V. (2020). An Improved Result on H_∞ Load Frequency Control for PSs with Time Delays. *IEEE Systems Journal*, *15*(3), 3238-3248.

[22] Annamraju, A., Babu, P. V., Repalle, S. R., Srinivasarathnam, C., Naik, P. L., & Salkuti, S. R. (2024). Coordinated Control Strategy for LFC in an Islanded Microgrid: A JAYA Algorithm Based Cascade PD-PI Approach. In *Energy and Environmental Aspects of Emerging Technologies for Smart Grid* (pp. 125-143). Cham: Springer International Publishing.

[23] Ekinci, S., Izci, D., Can, O., Bajaj, M., & Blazek, V. (2024). Frequency regulation of PV-reheat thermal PS via a novel hybrid educational competition optimizer with pattern search and cascaded PDN-PI controller. *Results in Engineering*, *24*, 102958.

[24] Fathy, A., Yousri, D., Rezk, H., Thanikanti, S. B., & Hasanien, H. M. (2022). A robust fractional-order PID controller based load frequency control using modified hunger games search optimizer. *Energies*, *15*(1), 361.

[25] Amiri, F., & Moradi, M. H. (2023). Design of a new control method for dynamic control of the two-area microgrid: F. Amiri and MH Moradi. Soft Computing, 27(10), 6727-6747.

[26] Sambariya, D. K., Nagar, O., & Sharma, A. K. (2020). Application of FOPID design for LFC using flower pollination algorithm for three-area PS. *Univers. J. Contr. Autom*, *8*, 212695735.

[27] Ding, J., Wang, J., Shi, K., & Cai, X. (2024). TS Fuzzy Sampled-Data LFC Scheme for Wind PS via Improved Trapezoidal Algorithm. *IEEE Transactions on Automation Science and Engineering*.

[28] Nireekshana, N., Ramachandran, R., & Narayana, G. V. (2024). An innovative fuzzy logic frequency regulation strategy for two-area PSs. *International Journal of Power Electronics and Drive Systems (IJPEDS)*, *15*(1), 603-610.

[29] Daood, O., Najeeb, M., & Ali, I. I. (2024). An Efficient Load Frequency Control for Multiple PSs Using Fuzzy Logic-Proportional Integral Derivative Controller. *International Journal of Electrical and Electronics Research*, *12*(2), 654-661.

[30] Guo, J. (2024). A Novel Proportional-Derivative Sliding Mode for Load Frequency Control. IEEE Access.

[31] Shutnan, W. A., Mohammed, N. A., Abdulmunem, F. A., Najim, A. H., Hassan, M. Y., Soliman, N. F., & Algarni, A. D. (2024). Modeling and Control of A 3DOF Robot Manipulator Using Artificial Fuzzy-Immune FOPID Controller. IEEE Access.

[32] Zaki, H., Rashid, A., & Masud, U. (2024). Lyapunov-based fractional-order PID controller design for coupled nonlinear system. Transactions of the Institute of Measurement and Control, 01423312241262067.

[33] Jegatheesh, A., Thiyagarajan, V., Selvan, N. M., & Raj, M. D. (2024). Voltage regulation and stability enhancement in AVR system based on SOA-FOPID controller. Journal of Electrical Engineering & Technology, 19(1), 31-44.

[34] Riad, A. J., Hasanien, H. M., Ullah, Z., Alkuhayli,

A., & Yakout, A. H. (2024). Voltage control of PEM fuel cell in a DC microgrid using optimal artificial rabbits algorithm-based fractional order PID controller. IEEE Access.

[35] Sahin, A. K., Cavdar, B., & Ayas, M. S. (2024). An adaptive fractional controller design for automatic voltage regulator system: sigmoid-based fractional-order PID controller. Neural Computing and Applications, 1-23.

[36] Mohamed, M. J., & Thamir Rasheed, L. (2024). Design of Nonlinear PID and FOPID Controllers for Electronic Throttle Valve Plate's Position. Journal of Electrical and Computer Engineering, 2024(1), 9984750.

[37] Jalali Khalil Abadi, Z., & Mansouri, N. (2024). A comprehensive survey on scheduling algorithms using fuzzy systems in distributed environments. Artificial Intelligence Review, 57(1), 4.

[38] Gu, X., Han, J., Shen, Q., & Angelov, P. P. (2023). Autonomous learning for fuzzy systems: a review. Artificial Intelligence Review, 56(8), 7549-7595.

[39] Luo, F. M., Xu, T., Lai, H., Chen, X. H., Zhang, W., & Yu, Y. (2024). A survey on model-based reinforcement learning. Science China Information Sciences, 67(2), 121101.

[40] Ji, J., Zhou, J., Zhang, B., Dai, J., Pan, X., Sun, R., ... & Yang, Y. (2024). Omnisafe: An infrastructure for accelerating safe reinforcement learning research. Journal of Machine Learning Research, 25(285), 1-6.

[41] Margolis, G. B., Yang, G., Paigwar, K., Chen, T., & Agrawal, P. (2024). Rapid locomotion via reinforcement learning. The International Journal of Robotics Research, 43(4), 572-587.

[42] Perera, A. T. D., & Kamalaruban, P. (2021). Applications of reinforcement learning in energy systems. Renewable and Sustainable Energy Reviews, 137, 110618.

Biography

Farhad Amiri was born in Ilam. He received his MSc and PhD degrees in electrical engineering in 2017 and 2022, respectively, from Bu-Ali Sina University. He also received his post-doctoral (Electrical engineering) in 2024 from the National Elites Foundation of Iran. His research interests include dynamic and transient performance of power system, control, Microgrid and renewable energy.

Mohammad Hassan Moradi was born in Nowshahr, Mazandaran, Iran. He obtained his B.Sc., M.Sc. and PhD from Sharif University of Technology, Tarbiat Modares University and Strathclyde University in Glasgow, Scotland in 1991 1993 and 2002 respectively. His research interests include New and Green Energy, Microgrid Modeling and Control, DG Location and Sizing in Power System, photovoltaic systems and power electronics, Combined Heat and Power Plant, Power Quality, Supervisory Control, Fuzzy Control.

Arefe Shalbafian was born in Bahar, Hamedan, Iran. She received the B.Sc., M.Sc., and Ph.D. degrees in electrical engineering from Bu-Ali Sina University, Iran. Her current research interests include robust control, adaptive control, nonlinear control, optimal control, and renewable energy systems.